Experimental Validation of Robust Chatter Control for High-Speed Milling Processes

van de Wouw, Nathan; van Dijk, N.J.M.; Schiffler, A.; Nijmeijer, Henk; Abele, E.

DOI
10.1007/978-3-319-53426-8_21

Publication date
2017

Document Version
Final published version

Published in
Time Delay Systems

Citation (APA)
van de Wouw, N., van Dijk, N. J. M., Schiffler, A., Nijmeijer, H., & Abele, E. (2017). Experimental Validation of Robust Chatter Control for High-Speed Milling Processes. In T. Insperger, T. Ersal, & G. Orosz (Eds.), *Time Delay Systems: Theory, Numerics, Applications, and Experiments* (pp. 315-331). (Advances in Delays and Dynamics (ADVSDD); Vol. 7). Springer. https://doi.org/10.1007/978-3-319-53426-8_21

Experimental Validation of Robust Chatter Control for High-Speed Milling Processes

N. van de Wouw, N.J.M. van Dijk, A. Schiffler, H. Nijmeijer and E. Abele

Abstract This chapter presents results on the design and experimental implementation and testing of robust controllers for the high-speed milling process for the purpose of avoiding chatter vibrations. Chatter vibrations are intimately related to the delay nature of the cutting process inherent to milling and should be avoided to ensure a high product quality. A design approach based on μ-synthesis is used to synthesize a controller that avoids chatter vibrations in the presence of model uncertainties and while respecting key performance specifications. The experimental validation of this controller on a benchmark setup, involving a spindle system including an active magnetic bearing, shows that chatter can be robustly avoided while significantly increasing the material removal rate, i.e., the productivity.

N. van de Wouw (✉)
Department of Mechanical Engineering, Eindhoven University of Technology,
Eindhoven, The Netherlands
e-mail: N.v.d.Wouw@tue.nl

N. van de Wouw
Department of Civil, Environmental & Geo-Engineering, University of Minnesota,
Minneapolis, USA

N. van de Wouw
Delft Center for Systems and Extra Control, Delft University of Technology,
Delft, The Netherlands

N.J.M. van Dijk
Philips Innovation Services, Eindhoven, The Netherlands
e-mail: niels.van.dijk@philips.com

A. Schiffler
Schaeffler Technologies AG & Co. KG, Schweinfurt, Germany
e-mail: andreas.schiffler@schaeffler.com

H. Nijmeijer
Department of Mechanical Engineering, Eindhoven University of Technology,
Eindhoven, The Netherlands
e-mail: H.Nijmeijer@tue.nl

E. Abele
Institut Für Produktionsmanagement, Technologie und Werkzeugmaschinen,
Technische Universität Darmstadt, Darmstadt, Germany
e-mail: abele@ptw.tu-darmstadt.de

T. Insperger et al. (eds.), *Time Delay Systems*,
Advances in Delays and Dynamics 7, DOI 10.1007/978-3-319-53426-8_21

1 Introduction

Chatter is an instability phenomenon in machining processes. The occurrence of (regenerative) chatter results in an inferior workpiece quality due to heavy vibrations of the cutter. Moreover, a high noise level is produced, the tool wears out rapidly and damage to the spindle unit may be caused, inducing high manufacturing costs. The occurrence of chatter can be visualized in so-called stability lobes diagrams (SLD). In a SLD, the chatter stability boundary between a stable cut (i.e. without chatter) and an unstable cut (i.e. with chatter) is visualized in terms of spindle speed and depth of cut (two key parameters characterizing the productivity).

The present day manufacturing industry demands high-precision products manufactured at a high productivity rate. This feeds the desire for the design of dedicated control strategies, which are able to actively alter the chatter stability boundary such that a higher productivity becomes feasible while avoiding chatter.

Three distinct approaches exist in literature to control chatter. The first method involves adjusting process parameters (i.e. spindle speed, feed per tooth or chip load) such that a stable working point is chosen [7, 25]. Although chatter can be eliminated by adaptation of process parameters, this methodology does not enlarge the domain of stable operation points toward those of higher productivity. A second method is to disturb the regenerative (delay) effect by continuous spindle speed modulation, see [26, 30]. Although the stability boundary is altered by spindle speed modulation, see [15], the method cannot be used in the case of high-speed milling since the modulation speed is limited by the inertia and actuation power of the spindle. The third method is to passively or actively alter the machine dynamics to favorably shape the chatter boundary. There are passive chatter suppression techniques that use dampers ([20]) or vibration absorbers ([28]). Active chatter control in milling has mainly been focused on the active damping of machine dynamics, see [11, 19], or workpiece, see [31]. Damping the machine or workpiece dynamics, either passively or actively, results in a uniform increase of the stability boundary for all spindle speeds. To enable more dedicated shaping of the stability boundary (e.g. lifting the SLD locally around a specific spindle speed), the regenerative (delay) effect should be taken into account during chatter controller design. In [23], an optimal state feedback observer-controller combination with integral control in the case of turning was designed. Recently, Chen and Knospe [5] developed three different chatter control strategies in the case of turning: speed-independent control, speed-specified control, and speed interval control.

Recently, in [8, 9] an active chatter control strategy based μ-synthesis has been proposed with the following benefits. First, using this approach, controllers can be designed that guarantee chatter-free cutting operations in an a priori defined range of process parameters, such as the spindle speed and depth of cut. Second, the approach explicitly takes the regenerative (delay) effect, responsible for chatter, into account in the milling models serving as basis for controller design. Third, robust stabilization of high-speed milling operations is achieved in the presence of model uncertainties (regarding the spindle-tool dynamics), while minimizing the control effort needed.

In this chapter, we experimentally validate controllers designed using the approach in [8, 9] on an experimental benchmark setup equipped with Active Magnetic Bearings (AMB) in the spindle, also used in [18] for chatter control using active damping techniques. Section 2 presents the dynamic model of the milling process in the form of a nonlinear time-varying delay differential equation (DDE) and a simplified DDE model used in the scope of controller design is introduced. In Sect. 3, the experimental setup is described and the experimental identification of the model for the setup is discussed. Section 4 presents the controller design approach used and the resulting controller design for the experimental setup. Finally, experimental results are presented that illustrate the effectiveness of this chatter control approach to improve the material removal rate of the milling process while guaranteeing the avoidance of chatter. Section 5 concludes this chapter.

2 High-Speed Milling Process

2.1 Comprehensive Milling Model

A model of the milling process will be described below, see e.g., [3, 13, 17, 27] for more details. In Fig. 1, a schematic representation of the milling process is depicted. The predefined motion of the tool with respect to the workpiece is characterized in terms of the static chip thickness $h_{j,\mathsf{stat}}(t) = f_z \sin \phi_j(t)$, where f_z is the feed per tooth and $\phi_j(t)$ the rotation angle of the j-th tooth of the tool with respect to the y (normal) axis. However, the total chip thickness $h_j(t)$ also depends on the interaction between the cutter and the workpiece. This interaction causes cutter vibrations resulting in a dynamic displacement $\underline{v}_t(t) = \left[v_{t,x}(t)\, v_{t,y}(t)\right]^T$ of the tool, see Fig. 1, which is superimposed on the predefined tool motion and results in a wavy workpiece surface. The next tooth encounters this wavy surface, generated by the previous tooth, and, in turn, generates its own waviness. This is called the regenerative effect. The difference between the current and previous wavy surface generates the dynamic chip thickness, denoted by $h_{j,\mathsf{dyn}}(t) = \left[\sin \phi_j(t) \cos \phi_j(t)\right] \left(\underline{v}_t(t) - \underline{v}_t(t-\tau)\right)$ with $\tau = 60/(zn)$ the delay, z the number of teeth and n the spindle speed in revolutions per minute (rpm). Hence, the total chip thickness removed by tooth j at time t equals $h_j(t) = h_{j,\mathsf{stat}}(t) + h_{j,\mathsf{dyn}}(t)$. Here, a circular tooth path is assumed, while in reality the tooth path is trochoidal, see [14]. For high radial immersion cuts (such as the full immersion cuts considered here), the circular tool path model forms a good approximation, also in terms of the prediction of the chatter stability boundary, see [14].

The cutting force model relates the total chip thickness to the forces acting at the tool tip. The tangential and radial forces, F_t and F_r in Fig. 1, for a single tooth j, are described by the following exponential cutting force model:

$$F_{t_j}(t) = g_j\big(\phi_j(t)\big) K_t\, a_p\, h_j(t)^{x_F},\ F_{r_j}(t) = g_j\big(\phi_j(t)\big) K_r\, a_p\, h_j(t)^{x_F}, \tag{1}$$

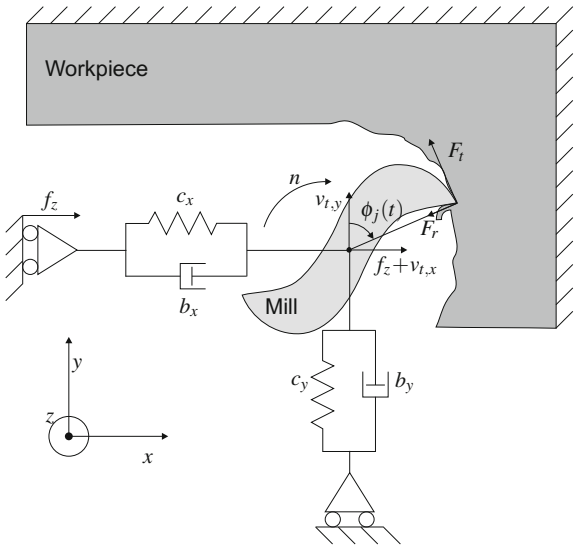

Fig. 1 Schematic representation of the milling process

where $0 < x_F \leq 1$ and $K_t, K_r > 0$ are cutting parameters which depend on the workpiece material. Moreover, a_p is the axial depth of cut. The function $g_j\big(\phi_j(t)\big)$ in (1) describes whether a tooth is in or out of cut:

$$g_j\big(\phi_j(t)\big) = \begin{cases} 1, & \phi_s \leq \phi_j(t) \leq \phi_e \wedge h_j(t) > 0, \\ 0, & \text{else}, \end{cases} \tag{2}$$

where ϕ_s and ϕ_e are the entry and exit angles of the cut, respectively. The total cutting forces in the x- and y-directions, $\underline{F}_t(t) = \left[F_{t,x}(t)\ F_{t,y}(t)\right]^T$, can be obtained by summing over all z teeth:

$$\begin{aligned} \underline{F}_t(t) = a_p \sum_{j=0}^{z-1} g_j\big(\phi_j(t)\big) \Big(\Big(& h_{j,\text{stat}}(t) \\ & + \left[\sin\phi_j(t)\ \cos\phi_j(t)\right]\big(\underline{v}_t(t) - \underline{v}_t(t-\tau)\big) \Big)^{x_F} \mathbf{S}_j(t) \begin{bmatrix} K_t \\ K_r \end{bmatrix} \Big) \end{aligned} \tag{3}$$

with $\mathbf{S}_j(t) = \begin{bmatrix} -\cos\phi_j(t) & -\sin\phi_j(t) \\ \sin\phi_j(t) & -\cos\phi_j(t) \end{bmatrix}$.

The cutting force interacts with the machine (spindle and tool) dynamics, which are modeled with a linear multi-input-multi-output (MIMO) state-space model,

$$\begin{aligned} \dot{\underline{x}}(t) &= \mathbf{A}\underline{x}(t) + \mathbf{B}_t\underline{F}_t(t) + \mathbf{B}_a\underline{F}_a(t), \\ \underline{v}_t(t) &= \mathbf{C}_t\underline{x}(t), \quad \underline{v}_a(t) = \mathbf{C}_a\underline{x}(t), \end{aligned} \tag{4}$$

where $\underline{x}(t)$ is the state. $\underline{F}_a(t) = \left[F_{a,x}(t)\ F_{a,y}(t)\right]^T$ denote the control forces, where $F_{a,x}(t)$ and $F_{a,y}(t)$ are the control forces acting in the x- and y-direction, respectively. Moreover, $\underline{v}_a(t)$ represents the measured displacements available for feedback (see Sect. 4).

Substitution of (3) into (4) results in the nonlinear, nonautonomous delay differential equations (DDE) describing the dynamics of the milling process:

$$\begin{aligned}\dot{\underline{x}}(t) &= \mathbf{A}\underline{x}(t) + \mathbf{B}_a\underline{F}_a(t) + \mathbf{B}_t a_p \sum_{j=0}^{z-1} g_j\big(\phi_j(t)\big)\Big(\Big(h_{j,\mathrm{stat}}(t) \\ &\quad + \left[\sin\phi_j(t)\ \cos\phi_j(t)\right]\mathbf{C}_t\big(\underline{x}(t) - \underline{x}(t-\tau)\big)\Big)^{x_F}\mathbf{S}(t)\begin{bmatrix}K_t\\K_r\end{bmatrix}\Big), \\ \underline{v}_a(t) &= \mathbf{C}_a\underline{x}(t).\end{aligned} \tag{5}$$

2.2 Stability of the Milling Process and Its Relation to Chatter

The static chip thickness $h_{j,\mathrm{stat}}(t)$ is periodic with period time $\tau = \frac{60}{zn}$. In general, the uncontrolled (i.e. $\underline{F}_a(t) \equiv 0$) milling model (5) has a periodic solution $\underline{x}^*(t)$ with period time τ, see [14]. In the absence of chatter, this periodic solution is (locally) asymptotically stable and when chatter occurs it is unstable. Hence, the chatter stability boundary can be analyzed by studying the (local) stability properties of the periodic solution $\underline{x}^*(t)$. Hereto, the milling model is linearized about the periodic solution $\underline{x}^*(t)$ for zero control input (i.e. $\underline{F}_a(t) \equiv 0$) yielding the following linearized dynamics in terms of perturbations $\tilde{\underline{x}}(t)$ ($\underline{x}(t) = \underline{x}^*(t) + \tilde{\underline{x}}(t)$):

$$\begin{aligned}\dot{\tilde{\underline{x}}}(t) &= \mathbf{A}\tilde{\underline{x}}(t) + a_p\mathbf{B}_t\sum_{j=0}^{z-1}\mathbf{H}_j(\phi_j(t))\mathbf{C}_t(\tilde{\underline{x}}(t) - \tilde{\underline{x}}(t-\tau)) + \mathbf{B}_a\underline{F}_a(t), \\ \tilde{\underline{v}}_a(t) &= \mathbf{C}_a\tilde{\underline{x}}(t),\end{aligned} \tag{6}$$

where

$$\mathbf{H}_j(\phi_j(t)) = g_j\big(\phi_j(t)\big)x_F(f_z\sin\phi_j(t))^{x_F-1}\mathbf{S}(t)\begin{bmatrix}K_t\\K_r\end{bmatrix}\begin{bmatrix}\sin\phi_j(t)\\\cos\phi_j(t)\end{bmatrix}^T. \tag{7}$$

The linearized model (6), (7) is a delayed, periodically time-varying system. As described in [3], for full immersion cuts it is sufficient to average the dynamic cutting forces $\sum_{j=0}^{z-1}\mathbf{H}_j(\phi_j(t))$ over the tool path such that the milling model becomes time-invariant. Since the cutter is only cutting when $\phi_s \le \phi_j \le \phi_e$ the averaged cutting forces are given by

$$\bar{\mathbf{H}} = \frac{z}{2\pi} \int_{\phi_s}^{\phi_e} \sum_{j=0}^{z-1} \mathbf{H}_j(\phi) \mathrm{d}\phi. \tag{8}$$

Then, a linear time-invariant model of the milling process is obtained by combining (6) with $\sum_{j=0}^{z-1} \mathbf{H}_j(\phi_j(t))$ replaced by $\overline{\mathbf{H}}$ and $\overline{\mathbf{H}}$ given in (8). The characteristic equation of the linear DDE (6), with $\sum_{j=0}^{z-1} \mathbf{H}_j(\phi_j(t))$ replaced by $\overline{\mathbf{H}}$ and $\overline{\mathbf{H}}$ given in (8), is then given as

$$\det(\mathbf{I} - a_p \mathbf{G}_{tt}(i\omega)\overline{\mathbf{H}}(1 - e^{-i\omega\tau})) = 0, \tag{9}$$

where $\mathbf{G}_{tt}(i\omega) = \mathbf{C}_t(i\omega\mathbf{I} - \mathbf{A})^{-1}\mathbf{B}_t$ represents the frequency response function (FRF) from cutting forces at the tooltip to tooltip displacements. The chatter stability boundary can be obtained by solving (9) for depth of cut a_p and delay τ as e.g. discussed in [3], see also [16].

2.3 Model Simplification for Control

In support of the usage of robust control synthesis techniques as in [8, 9], we construct a finite-dimensional model approximation using a Padé approximation (see also [5]). Hereto, the delayed (perturbation) tool vibrations $\underline{\tilde{v}}_t(t-\tau) = \mathbf{C}_t\tilde{q}(t-\tau)$ are approximated by Padé approximation denoted by $\tilde{v}_p(t)$, such that $\underline{\tilde{v}}_t(t-\tau) = \mathbf{C}_t\tilde{q}(t-\tau) \approx \underline{\tilde{v}}_p(t)$. The milling model in (6) with cutting force averaging, defined in (8), and Padé approximation is given as,

$$\begin{aligned}
\begin{bmatrix} \dot{\tilde{q}}(t) \\ \dot{\tilde{q}}_p(t) \end{bmatrix} &= \begin{bmatrix} \mathbf{A} + a_p\mathbf{B}_t\overline{\mathbf{H}}(\mathbf{C}_t - \mathbf{D}_p\mathbf{C}_t) & -a_p\mathbf{B}_t\overline{\mathbf{H}}\mathbf{C}_t \\ \mathbf{B}_p\mathbf{C}_t & \mathbf{A}_p \end{bmatrix} \begin{bmatrix} \tilde{q}(t) \\ \tilde{q}_p(t) \end{bmatrix} + \begin{bmatrix} \mathbf{B}_a \\ \mathbf{0} \end{bmatrix} \underline{F}_a(t), \\
\underline{\tilde{v}}_a(t) &= \mathbf{C}_a\underline{\tilde{q}}(t),
\end{aligned} \tag{10}$$

where $\mathbf{A}_p, \mathbf{B}_p, \mathbf{C}_p$ and $\mathbf{D}_p$ denote matrices of the state-space description of the Padé approximation (with state $\tilde{q}_p(t)$). The order of the Padé approximation will be based on a desired level of accuracy regarding the predicted chatter stability boundary using the model with Padé approximation, see [9].

In the next section, the experimental identification of the milling model introduced above will be discussed. Subsequently, the following steps in model identification will be pursued: (1) the identification of the cutting model the spindle-tool dynamics, i.e., the parameters K_t, K_r and X_F in (7), (2) the identification of the spindle-tool dynamics, i.e., the matrices A, B_t, B_a, C_t and C_a in (4) and (3) the identification of uncertainties in these spindle-tool dynamics (needed in support of the design of chatter controllers that are robust in the presence of such uncertainties that are unavoidable in practice).

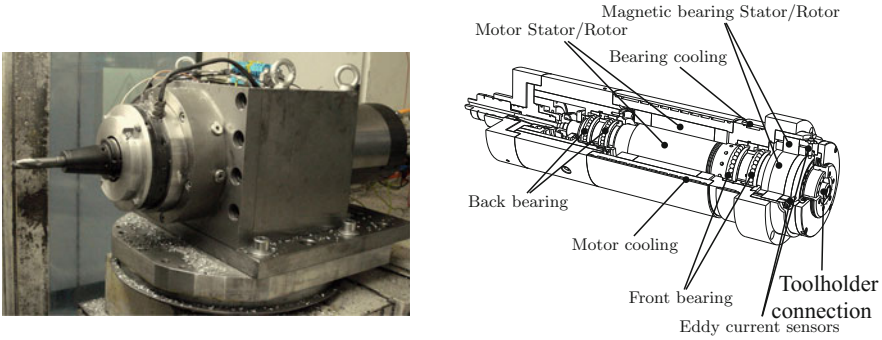

(a) Photo. (b) Schematic representation.

Fig. 2 The experimental setup. An active magnetic bearing (AMB) is integrated into a machine spindle between the front bearings and toolholder connection. *Source* Institut für Produktionsmanagement, Technologie und Werkzeugmaschinen (PTW), Technische Universität Darmstadt, Germany

3 Experimental Setup and Model Identification

3.1 Experimental Setup

The experimental setup, used in this chapter, is designed and realized at the Institut für Produktionsmanagement, Technologie und Werkzeugmaschinen (PTW) of the Technische Universität Darmstadt, Germany. In Fig. 2, a photo and schematic overview of the spindle with integrated Active Magnetic Bearing (AMB) can be found. It can be seen that the active magnetic bearing, to be used as actuator, is integrated in the spindle and is placed between the front bearings and the toolholder. Moreover, two eddy current sensors are employed to measure the spindle shaft motion relative to the spindle housing. In this way, the setup can serve as a testbed for a proof of principle in order to test the active chatter control strategy in practice. The specifications of the spindle and AMB, taken from [18], are listed in Table 1. The same spindle with integrated AMB has been used in [18] for chatter control using active damping techniques.

3.2 Identification of the Experimental Setup

In this section, we first concisely describe the result of experiments aiming at the identification of (1) the parameters of the cutting force model, (2) a parametric model of the spindle and actuator dynamics and (3) uncertainties in the spindle dynamics, see [6] for details. Next, the SLD of the experimental setup will be determined

Table 1 Specifications of the experimental setup

Spindle		AMB	
max. Power	80 kW	Number of poles	8
max. spindle speed	24,000 rpm	Nominal airgap	0.4 mm
		Pre-magnetizing current	5 A
		max. input current	10 A
		max. static force	600 N
		Bandwidth current controller	1000 Hz

through dedicated milling experiments as well as using the obtained model for the purpose of model validation.

Identification of the cutting force model parameters. Cutting tests have been performed to experimentally identify the parameters, K_t, K_r and x_F of the cutting force model (3). Hereto, full immersion cuts in aluminum 7075 have been performed while measuring the cutting forces using a dynamometer. The parameters are obtained by fitting the model on the experimentally obtained cutting forces in feed and normal direction using least squares optimization as outlined in [12]. The corresponding parameters are given by $K_t = 585.00$ N/mm$^{1+x_f}$, $K_r = 210.04$ N/mm$^{1+x_f}$ and $x_F = 0.7654$.

Identification of the spindle-actuator dynamics. Next, the nominal model of the spindle and actuator dynamics is determined experimentally. The model consists of four inputs (the input voltage to the current controller which drives the AMB and the force acting at the tooltip in feed (x)- and normal (y)-direction) and four outputs (displacements in feed (x)- and normal (y)-direction measured at the AMB location and the tooltip). In order to determine the frequency response functions (FRF), corresponding to this input/output set, the tooltip is excited using an impulse hammer while the accelerations at the tooltip are measured using an accelerometer and AMB displacements are measured using the eddy current sensors. The FRF matrix $\mathbf{G}$ of the spindle dynamics is defined as follows:

$$\mathbf{G}(i\omega) = \begin{bmatrix} \mathbf{G}_x(i\omega) & \mathbf{0} \\ \mathbf{0} & \mathbf{G}_y(i\omega) \end{bmatrix}, \text{ with } \mathbf{G}_\alpha(i\omega) = \begin{bmatrix} \mathbf{G}_{tt,\alpha}(i\omega) & \mathbf{G}_{ta,\alpha}(i\omega) \\ \mathbf{G}_{at,\alpha}(i\omega) & \mathbf{G}_{aa,\alpha}(i\omega) \end{bmatrix} \tag{11}$$

and $\alpha \in \{x, y\}$. Herein, $\mathbf{G}_{kl,x}(i\omega)$ (and $\mathbf{G}_{kl,y}(i\omega)$) denote the FRF with output $k \in \{a, t\}$ and input $l \in \{a, t\}$, where t and a indicate tooltip and bearing excitation/response, respectively. All the experiments are conducted at standstill. It is well-known that the spindle dynamics is generally dependent on the spindle speed [1, 21]. Such spindle speed dependency of the dynamics of experimental setup will be modeled by including uncertainty in the spindle-actuator dynamics model, see below. Based on the measured data, a parametric model is fitted to the obtained

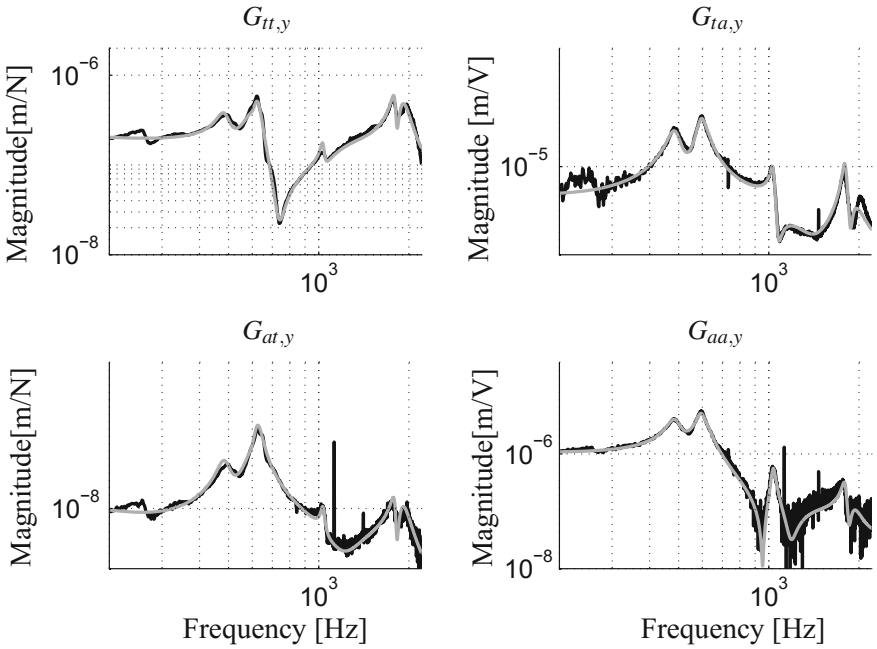

Fig. 3 Frequency response measurements (*black*) and fitted parametric model (*gray*) in normal (y) direction

frequency response functions. The multivariable model is described using polynomial matrix fraction descriptions ([4]). The parameters of the model are determined using Sanathanan–Koerner (SK) iteration, see [22].

In Fig. 3, the amplitude of the measured frequency response functions (FRFs) and corresponding parametric models in normal (y)-direction is given (information on the FRFs in the feed (x)-direction can be found in [6]). Especially near resonances, the fitted frequency response data and experimental data are quite comparable. The presented parametric model has a total of 30 states (14 in feed direction and 16 states in normal direction).

Identification of spindle-actuator dynamics uncertainties. To support the design of controllers that are robust for uncertainties in the milling machine dynamics, such uncertainties are identified here for the experimental setup under study. [12] concludes that the sensitivity of the SLD with respect to the spindle dynamics is considerably larger than the sensitivity to the parameters of the cutting force model. Consequently, during the controller design, uncertainties in the spindle-actuator model will be included. The following key sources of uncertainties in the model of the spindle-actuator dynamics are recognized: (1) uncertainty due to spindle speed dependent dynamics, (2) uncertainty due to unmodeled dynamics.

First, the uncertainty due to spindle speed dependent dynamics arises due to gyroscopic effects in the rotor and the spindle speed dependent bearing stiffness, see [21],

which results in a change of the low-frequent stiffness and a change in the eigenfrequencies of the spindle-actuator dynamics. The change in the low-frequency stiffness is compensated for by scaling the nominal model of the spindle-actuator dynamics. The associated scaling factor is determined by dividing the average value of the magnitude of the measured FRF $\mathbf{G}_{aa,k,n}$ (which is the only FRF from (11) that can be measured for a rotating spindle) from input voltage of the current controller to measured displacements $\underline{v}_a(t)$ at spindle speed n by the average value of magnitude of the FRF $\mathbf{G}_{aa,k,0}$ measured at standstill over a certain frequency range.

Second, in order to deal with changing eigenfrequencies due to spindle speed induced uncertainty (mainly due to changing bearing stiffness [1, 2, 21]), parametric uncertainties will be used to consider uncertain spindle modes. Here, uncertainty in the resonances is modeled as a parametric uncertainty in the eigenfrequencies of the associated resonances, see [6, 18]. Moreover, the uncertainty due to unmodeled dynamics is mainly due to the limited order of the parametric model which results in a deviation between the measured and modeled FRFs at higher frequencies. Moreover, at high frequencies the signal-to-noise ratio of the eddy current sensors becomes small, as can be seen from the measured FRFs in Fig. 3. Therewith, the structure of the model at high frequencies is unknown and the uncertainty is modeled using a (frequency-dependent) dynamic additive uncertainty.

In order to determine the uncertainties in the spindle-actuator dynamics of the experimental setup, FRFs from AMB input voltage to eddy current displacements $\underline{v}_a(t)$ have been measured for several spindle speeds. In this case, only the response at the bearing location can be measured. In Fig. 4, the amplitudes of the measured FRFs in feed and normal direction are given for several spindle speeds. This figure shows that there indeed is a significant change in the stiffness due to the spindle speed dependent dynamics. From now on, when a reference to the nominal model is made, it implies the model in which the scaling is absorbed. Figure 4 also shows that the first bending mode (which lies around 550 Hz) shifts as a function of the spindle speed. The gray area in this figure shows the uncertainty model for uncertainties on the resonances. Moreover, it can be seen that especially at frequencies above approximately 800 Hz the structure of the model (which is determined using measured data

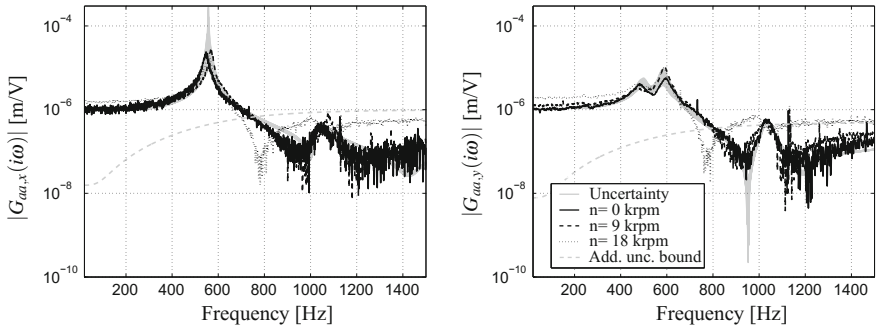

(a) feed direction. (b) normal direction.

Fig. 4 Frequency response data for bearing excitation experiments for several spindle speeds and uncertainty modeling

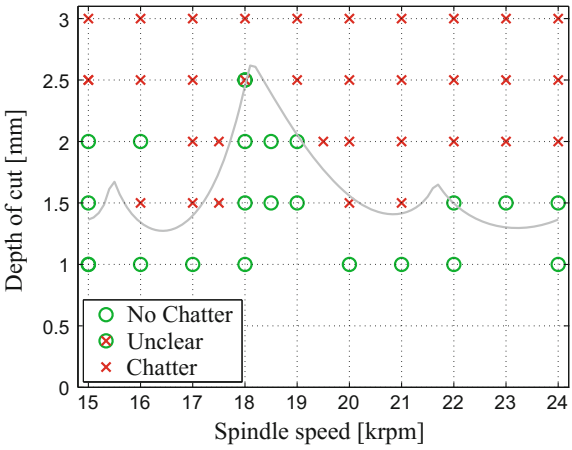

Fig. 5 Experimental (*o,x*) and (nominal) model-based (*gray line*) stability lobes diagram of the experimental setup

at standstill) does not match the measured FRFs. Based on these results, we model the uncertainties on the eigenfrequencies around 550 Hz by parametric uncertainties and add an additive uncertainty, see Fig. 4, to cope with the differences observed at higher frequencies. The measured spindle speed dependent spindle-actuator dynamics clearly lie inside the uncertainty set of the uncertain model of the spindle-actuator model.

3.2.1 Stability Lobes Diagram

First, stability lobes diagrams (SLD) are calculated using the open-loop linearized non autonomous model of the milling process (6) for the obtained parameters for the cutting force model and the *nominal* scaled parametric models of the spindle-actuator dynamics as presented above. The SLD is also determined experimentally. Hereto, cuts in aluminum 7075 have been made with the experimental setup as described in Sect. 3.1 for several spindle speeds and depth of cuts. Based on a visible inspection of the workpiece and the observed sound during the cut, a cut is marked with or without chatter. The resulting experimentally obtained SLD and the model-based SLD, calculated using the semi-discretization method ([16]), are presented in Fig. 5. It can be seen that the calculated SLD fits sufficiently well to the experimentally obtained SLD.

4 Control Approach and Validation

In this section, first a high-level description of the adopted chatter control approach will be given and next experimental results obtained with this approach will be presented.

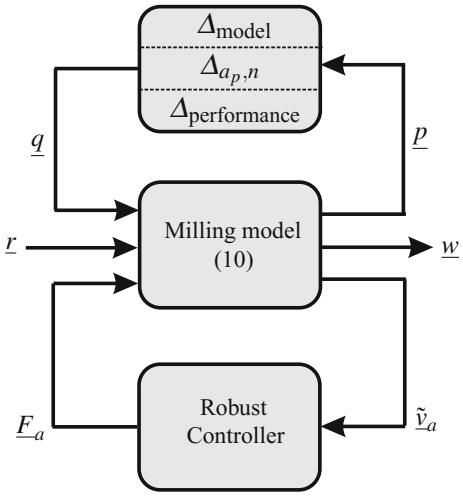

Fig. 6 Generalized plant framework, including uncertainties, used for controller synthesis

4.1 Chatter Control Approach

We employ the approach described in [8, 9] to design robust chatter controllers; for the sake of brevity only a high-level description of the approach is provided here.

In support of controller synthesis, a generalized plant framework as depicted in Fig. 6 is used. The main goal of the controller to be designed is to stabilize the dynamics (10), which implies that absence of chatter vibrations (at least locally). Figure 6 expresses that the controller used measured outputs $\underline{\tilde{v}}_a$, being the perturbation displacements in the active magnetic bearing. As the perturbation variants of these displacements cannot be directly measured, an online estimation algorithm for $\underline{\tilde{v}}_a$ as presented in [7] is used. The controller produces the forces $\underline{F}_a$ applied in the AMB. The uncertainty block consists of three parts: (1) Δ_{model} reflects the model uncertainty as identified in Sect. 3.2, (2) $\Delta_{a_p,n}$ reflects an uncertainty in the depth of cut a_p and the spindle speed n, which ensures that the controller stabilizes the milling process for an entire range of these parameters, and (3) $\Delta_{\text{performance}}$ embeds performance specifications for the controller, see [24], mainly related to limiting the control sensitivity, which in turn guarantees the limitation of the required control action. $\underline{p}$ and q represent an input–output pair needed in the interconnection between the plant dynamics and the uncertainty models. Finally, $\underline{r}$ reflects disturbances and measurement noise, while the performance output $\underline{z}$ represents the (weighted) control action. Now, a μ-synthesis approach, as proposed in [8, 9], is used to design linear, dynamic controllers that guarantee robustness with respect to these uncertainties.

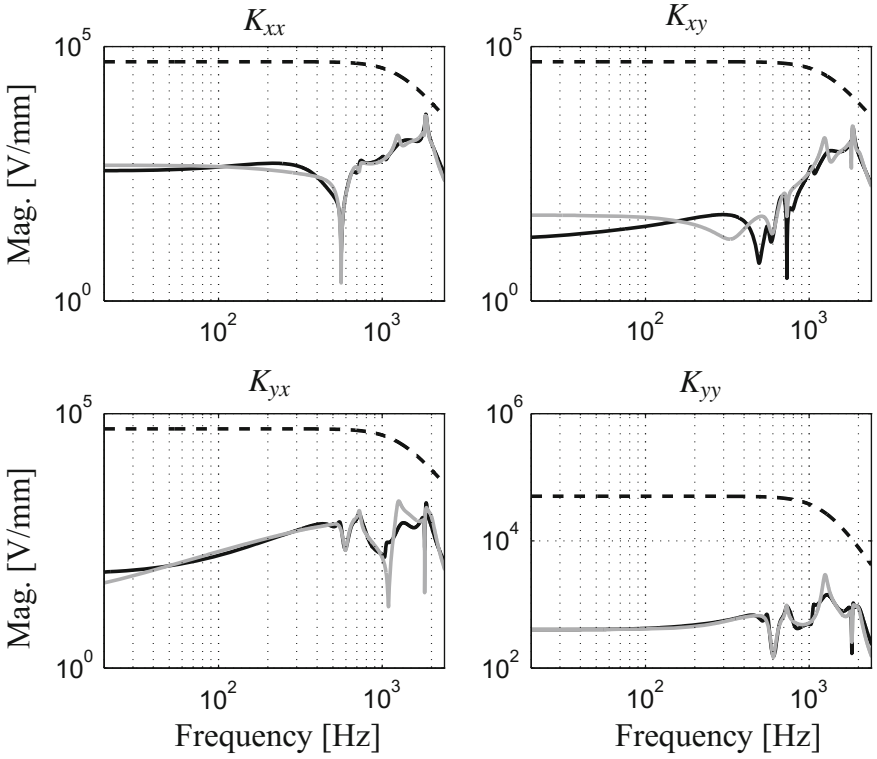

Fig. 7 Magnitude of the FRF for the full-order (*black*) and reduced-order (*gray*) controllers along with the inverse of the performance weighting function (*dashed*)

4.2 Chatter Controller Design

The SLD of the uncontrolled system in Fig. 5 shows that the productivity of the system measured in terms of the material removal rate (MMR) can be significantly increased when the critical depth of cut a_p is increased in the spindle speed range above 20,000 rpm. To this end, a controller for a single spindle speed of $n = 23{,}000$ rpm has been designed. The controller is designed by employing D-K-iteration with a bisection scheme to find the largest depth of cut $\overline{a}_p$ such that robust stability and performance is guaranteed. This yields a 98-th order controller that guarantees robust stability up to a depth of cut $\overline{a}_p = 2$ mm. Closed-loop model reduction yields a 19-th order controller for which robust stability and performance is still guaranteed up to $\overline{a}_p = 2$ mm. Magnitude plots of the high-order and reduced-order controllers are given in Fig. 7. It can be seen that the resulting controllers exhibit highly dynamical characteristics.

Next, closed-loop SLD diagrams are determined using the nominal linearized nonautonomous model of the milling model in (5) and the controller obtained above. The resulting closed-loop model-based SLDs along with the open-loop and

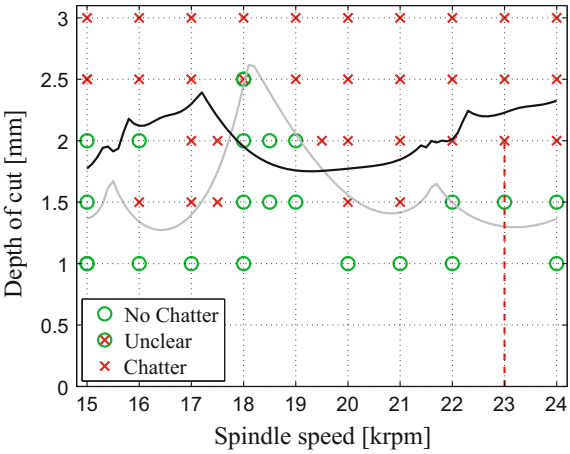

Fig. 8 Experimental (o, x) SLD and model-based (*solid lines*) SLD of the open-loop system (*gray*) and the closed-loop system for the reduced-order controller (*black*) using the nominal spindle dynamics

experimentally obtained SLD, as already presented in Sect. 3.2.1, are given in Fig. 8. The domain of stable operating points (in terms of the depth of cut) as guaranteed by the μ-synthesis is (for the model) given by the vertical dashed line: $\overline{a}_p = 2$ mm. The maximum achievable depth of cut (as obtained through computation of the SLD is given by $a_{p,max} = 2.23$ mm, as opposed to $a_{p,max} = 1.3$ mm for the open-loop case, which implies an increase of more than 70% in depth of cut.

4.3 Experimental Results

The robust controller, presented above, has been implemented and tested on the experimental setup. Before the results from a milling test are presented, first measurements are performed to determine the process sensitivity FRF of the closed-loop system in both feed and normal direction. The obtained FRFs are compared to measurements of the open-loop plant. Hereto, the AMB is excited using a 'pseudo-random binary sequence' signal, for a rotating spindle at $n = 23{,}000$ rpm while measuring the response using the eddy current sensors. The resulting magnitudes of the FRFs in feed and normal direction are given in Fig. 9.[1] From these figures, it can be concluded that the controller alters the spindle dynamics, where the first bending mode of the spindle is damped (especially in the normal direction) and a resonance is created at approximately 1510 Hz which is close to the second harmonic of the tooth passing excitation frequency ($2f_{tpe} = 2 \cdot \frac{2 \cdot 23{,}000}{60} \approx 1533$ Hz). As shown in [9], this characteristic of the closed-loop dynamics induces the raising of the SLD at the desired spindle speed (in this case 23,000 rpm), see Fig. 8.

Next, a full immersion cutting test has been performed at 23,000 rpm for a depth of cut of 2.5 mm using the controller with spindle-actuator uncertainty included in the controller design. Notice that chatter occurs for the open-loop at this depth of

[1]Note that in this case the tooltip dynamics, which are of interest for calculating the SLD, cannot be measured since the spindle is rotating.

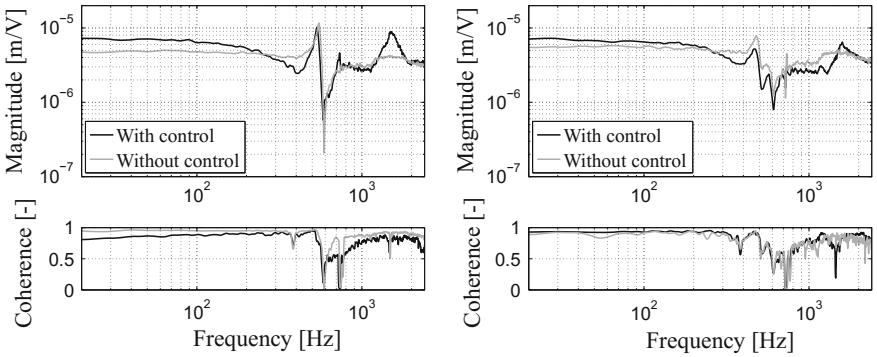

Fig. 9 Magnitude and coherence of the measured closed-loop process sensitivity and open-loop FRF from current controller input voltage to measured bearing displacements for $n = 23{,}000$ rpm

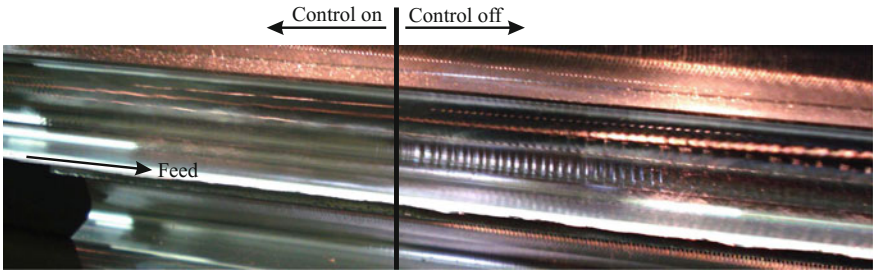

Fig. 10 Photo of the workpiece for an experiment at $n = 23{,}000$ rpm for a depth of cut of $a_p = 2.5$ mm, where in the first part of the cut the controller is on and is switched off after approximately 100 mm

cut, see Fig. 5. At the start of the cut, the controller is switched on. When the cutter is approximately 100 mm inside the material (in feed direction), the controller is switched off. After switching the controller off, chatter marks become visible on the workpiece. A picture of a part of the resulting workpiece is given in Fig. 10. It can be seen that, at the start of the cut, no chatter marks are visible on the workpiece, whereas chatter marks appear on the workpiece when the controller has been switched off.

Summarizing, it can be said that the working principle of the active chatter control design methodology has been illustrated in practice. With active chatter control for a single spindle speed, the depth of cut could be increased to 2.5 mm which is an increase of approximately 66% as compared to the experimentally uncontrolled obtained SLD in Fig. 5 at the same spindle speed.

5 Conclusions

This chapter has presented results on the experimental validation of an active control strategy for the avoidance of chatter vibrations in the high-speed milling process. In particular, a recently proposed robust control strategy [8, 9] has been tested on an experimental setup of a spindle with integrated Active Magnetic Bearing (AMB). The experimental results illustrate the effectiveness of the controller to robustly stabilize the milling process (i.e., avoid chatter) in the presence of significant model uncertainty and to achieve a significantly higher material removal rate while avoiding chatter.

Further research is needed on the following topics to promote the adoption of these techniques in industrial practice: (1) the development of robust online estimation techniques for chatter or alternatively the development of output feedback control techniques that do not need the estimation of the chatter (perturbation) vibrations, but can function with full vibrational measurements in the spindle, see e.g., [10, 29], and (2) further industrial development of active spindle systems including sensing and actuation techniques supporting the control techniques validated here.

Acknowledgements This work was supported by the Dutch Ministry of Economic affairs within the framework of Innovation Oriented Research Programmes (IOP) Precision Technology. We also thank E. J. J. Doppenberg and J. A. J. Oosterling (TNO Science and Industry, The Netherlands) for fruitful discussion on the topic of this research.

References

1. Abele, E., Kreis, M., Roth, M.: Electromagnetic actuator for in process non-contact identification of spindle-tool frequency respons functions. In: CIRP 2nd International Conference on High Performance Cutting, Vancouver, Canada, paper no. 103 (2006)
2. Abele, E., Schiffler, A., Rothenbücher, S.: System identification during milling via active magnetic bearing. Prod. Eng. Res. Dev. **1**(3), 309–314 (2007)
3. Altintas, Y.: Manufacturing Automation. Cambridge University Press, Cambridge, UK (2000)
4. de Callafon, R., de Roover, D., Van den Hof, P.: Multivariable least squares frequency domain identification using polynomial matrix fraction descriptions. In: Proceedings of the 35th IEEE Conference on Decision and Control, Kobe, Japan, vol. 2, pp. 2030–2035 (1996)
5. Chen, M., Knospe, C.R.: Control approaches to the suppression of machining chatter using active magnetic bearings. IEEE Trans. Control Syst. Technol. **15**(2), 220–232 (2007)
6. van Dijk, N.: Active chatter control in high-speed milling processes. PhD thesis, Eindhoven University of Technology. http://www.dct.tue.nl/New/Wouw/phdthesisvandijk2011.pdf (2011)
7. van Dijk, N.J.M., Doppenberg, E.J.J., Faassen, R.P.H., van de Wouw, N., Oosterling, J.A.J., Nijmeijer, H.: Automatic in-process chatter avoidance in the high-speed milling process. J. Dyn. Syst. Meas. Control **132**(3), 031,006 (14 pp) (2010a)
8. van Dijk, N.J.M., van de Wouw, N., Doppenberg, E.J.J., Oosterling, J.A.J., Nijmeijer, H.: Chatter control in the high-speed milling process using μ-synthesis. In: Proceedings of the American Control Conference, pp. 6121–6126, Baltimore, MD, USA (2010b)

9. van Dijk, N.J.M., van de Wouw, N., Doppenberg, E.J.J., Oosterling, J.A.J., Nijmeijer, H.: Robust active chatter control in the high-speed milling process. IEEE Trans. Control Syst. Technol. **20**(4), 901–917 (2012)
10. van Dijk, N.J.M., van de Wouw, N., Nijmeijer, H.: Fixed-structure robust controller design for chatter mitigation in high-speed milling. Int. J. Robust Nonlinear Control **25**(17), 34953514 (2015)
11. Dohner, J.L., Lauffer, J.P., Hinnerichs, T.D., Shankar, N., Regelbrugge, M.E., Kwan, C.M., Xu, R., Winterbauer, B., Bridger, K.: Mitigation of chatter instabilities in milling by active structural control. J. Sound Vib. **269**(1–2), 197–211 (2004)
12. Faassen, R.: Chatter prediction and control for high-speed milling: Modelling and experiments. PhD thesis, Eindhoven University of Technology (2007)
13. Faassen, R.P.H., van de Wouw, N., Oosterling, J.A.J., Nijmeijer, H.: Prediction of regenerative chatter by modelling and analysis of high-speed milling. Int. J. Mach. Tools Manuf. **43**(14), 1437–1446 (2003)
14. Faassen, R.P.H., van de Wouw, N., Nijmeijer, H., Oosterling, J.A.J.: An improved tool path model including periodic delay for chatter prediction in milling. J. Comput. Nonlinear Dyn. **2**(2), 167–179 (2007)
15. Insperger, T., Stépán, G.: Stability analysis of turning with periodic spindle speed modulation via semi-discretisation. J. Vib. Control **10**, 1835–1855 (2004)
16. Insperger, T., Stépán, G.: Updated semi-discretization method for periodic delay-differential equations with discrete delay. Int. J. Num. Methods Eng. **61**(1), 117–141 (2004)
17. Insperger, T., Stépán, G., Bayly, P.V., Mann, B.P.: Multiple chatter frequencies in milling processes. J. Sound Vib. **262**(2), 333–345 (2003)
18. Kern, S.: Erhöhung der prozessstabilität durch aktive dämpfung von frässpindeln mittels elektromagnetischer aktoren. PhD thesis, Technische Universität Darmstadt, Darmstadt, Germany (2009)
19. Kern, S., Ehmann, C., Nordmann, R., Roth, M., Schiffler, A., Abele, E.: (2006) Active damping of chatter vibrations with an active magnetic bearing in a motor spindle using μ-synthesis and an adaptive filter. In: The 8th International Conference on Motion and Vibration Control
20. Liu, K.J., Rouch, K.E.: Optimal passive vibration control of cutting process stability in milling. J. Mater. Process. Technol. **28**(1–2), 285–294 (1991)
21. Rantatalo, M., Aidanpä, J., Göransson, B., Norman, P.: Milling machine spindle analysis using fem and non-contact spindle excitation and response measurement. Int. J. Mach. Tools Manuf. **47**(7–8), 1034–1045 (2007)
22. Sanathanan, C., Koerner, J.: Transfer function synthesis as a ratio of two complex polynomials. IEEE Trans. Autom. Control **8**(1), 56–58 (1963)
23. Shiraishi, M., Yamanaka, K., Fujita, H.: Optimal control of chatter in turning. Int. J. Mach. Tools Manuf. **31**(1), 31–43 (1991)
24. Skogestad, S., Postlethwaite, I.: Multivariable Feedback Control: Analysis and Design, 2nd edn. Wiley, Chichester (2005)
25. Smith, S., Delio, T.: Sensor-based chatter detection and avoidance by spindle speed. J. Dyn. Syst. Meas. Control **114**(3), 486–492 (1992)
26. Soliman, E., Ismail, F.: Chatter suppression by adaptive speed modulation. Int. J. Mach. Tools Manuf. **37**(3), 355–369 (1997)
27. Stépán, G.: Modelling nonlinear regenerative effects in metal cutting. Philos. Trans. R. Soc. A: Math. Phys. Eng. Sci. **359**(1781), 739–757 (2001). doi:10.1098/rsta.2000.0753
28. Tarng, Y.S., Kao, J.Y., Lee, E.C.: Chatter suppression in turning operations with a tuned vibration absorber. J. Mater. Process. Technol. **105**(1), 55–60 (2000)
29. van de Wouw, N., van Dijk, N.J.M., Nijmeijer, H.: Pyragas-type feedback control for chatter mitigation in high-speed milling. In: Proceedings of the A12th IFAC Workshop on Time Delay Systems, Ann-Arbor, MI, USA (2015)
30. Yilmaz, A., AL-Regib, E., Ni, J.: Machine tool chatter suppression by multi-level random spindle speed variation. J. Manuf. Sci. Eng. **124**(2), 208–216 (2002)
31. Zhang, Y., Sims, N.D.: Milling workpiece chatter avoidance using piezoelectric active damping: a feasibility study. Smart Mater. Struct. **14**(6), N65–N70 (2005)